NRL Formal Report 8345

Nonlinear Spectral Analysis and Adaptive Array Superresolution Techniques

William F. Gabriel

February 1, 1980

NAVAL RESEARCH LABORATORY
Washington, D.C.

20. Abstract (Continued)

spectrum estimators are suggested, consisting of a circular array predicting to its center point, and a new "thermal noise" algorithm.

CONTENTS

NONLINEAR SPECTRAL ANALYSIS AND ADAPTIVE ARRAY SUPERRESOLUTION TECHNIQUES

INTRODUCTION

Nonlinear spectral analysis techniques are currently of intense interest because of reported "superresolution" capabilities beyond the conventional periodogram or the Blackman-Tukey windowed Fourier transform [1]. Two methods, in particular, which have demonstrated a considerable increase in resolution are the maximum entropy spectral analysis (MESA) technique introduced by J. P. Burg [2,3], and the maximum likelihood method (MLM) demonstrated by J. Capon [4-6]. Since these techniques are most significant when processing short data sets, it is natural to consider their use for RF array antennas with a modest number of elements [7,8].

Adaptive processing techniques have been associated with these spectral estimation methods to some extent [9-11], but the literature indicates that cross-fertilization has been rather sparse. This situation is surprising, because both MESA and MLM bear a very close relationship to nonlinear adaptive array processing techniques. It is the purpose of this report to relate the MESA and MLM methods to their similar adaptive array antenna counterparts. The comparison analysis permits an examination of their principles of operation from the antenna array spatial pattern viewpoint, and helps to qualify their superresolution performance behavior. The real-time adaptive resolution of two incoherent sources located within a beamwidth has been simulated, and results are presented over an array output signal-to-noise ratio (SNR) range of 0 to 40 dB. The difficulties involved in resolving more than two closely spaced sources are also treated.

In addition to a discussion on the similarities between MESA, MLM, and adaptive array processing, some attention is given to the significant differences, which include the matter of two-dimensional data and the particular manner of averaging or estimating interelement signal correlations.

Alternate techniques for estimating spatial spectra have suggested themselves during the course of this study, and two of these are briefly described in the section on alternate adaptive processing (pp. 19, 20): phase center prediction utilizing a circular array, and a new adaptive "thermal noise" algorithm.

BURG MESA LINEAR PREDICTION FILTER

The Burg MESA method has been shown by van den Bos [12] to be equivalent to least mean square (LMS) error linear prediction. It runs a K-point linear prediction filter across a data sequence of N samples, where N should be at least twice the value of K. In the

Manuscript submitted July 24, 1979.

discrete filter diagram of Fig. 1, an optimum K-point prediction filter predicts the nth value of the sequence from K past values,

$$\hat{X}_n = \sum_{k=1}^{K} A_k X_{n-k}, \tag{1}$$

where $\hat{X}_n$ is the predicted sample, the A_k are optimum weighting coefficients, and the K past samples of X_{n-k} are presumed known. To define the difference between this predicted value and the current true value of X_n as the error ϵ_n, which is to be LMS minimized, we set

$$\epsilon_n = X_n - \hat{X}_n . \tag{2}$$

We minimize the total squared error E over the complete data sequence of N samples,

$$E = \sum_{n=K}^{N-1} \epsilon_n^2 \tag{3}$$

and

$$\frac{\partial E}{\partial A_i} = 0, \qquad 1 \leqslant i \leqslant K, \tag{4}$$

thus obtaining a set of K equations in K unknowns, i.e., the A_k filter weights,

$$\sum_{k=1}^{K} A_k \phi_{ki} = -\phi_{0i} \qquad \begin{matrix} 1 \leqslant k \leqslant K \\ 1 \leqslant i \leqslant K \end{matrix} \tag{5}$$

$$\phi_{ki} = \sum_{n=k}^{N-1} X_{n-k} X_{n-i} . \tag{6}$$

There are several different techniques, including Burg's, for manipulating this set of equations to solve for the optimum A_k filter weights, and Ref. 1 is recommended if the reader is interested in pursuing the details further. When this error has been minimized, its power spectrum will be equivalent to "white" noise. Thus, the uncertainty in ϵ_n has been maximized, hence we have a maximum entropy filter.

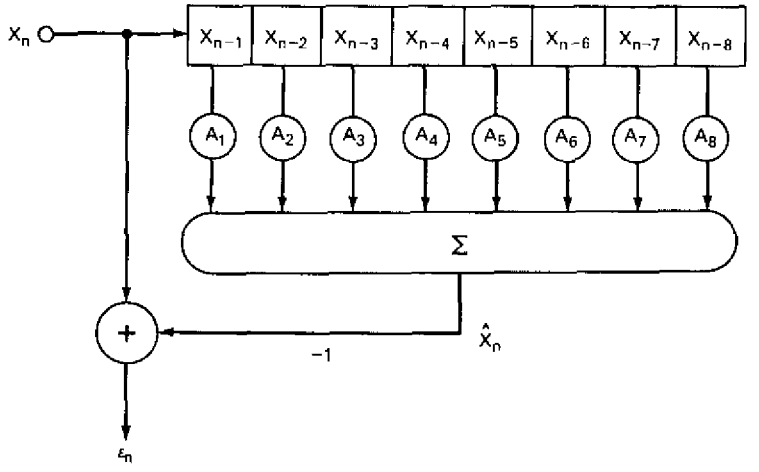

Fig. 1—Maximum-entropy filter with one-step linear prediction estimator

Upon substituting Eq. (1) into Eq. (2), we readily see that we have the form of a discrete convolution

$$\epsilon_n = - \sum_{k=0}^{K} A_k \, X_{n-k}, \tag{7}$$

where $A_o = -1$. The associated Z-transforms may be written,

$$\mathcal{E}(Z) = \left(1 - \sum_{k=1}^{K} A_k \, Z^{-k} \right) X(Z), \tag{8}$$

where the expression within the parentheses may be defined as the filter transform function $H(Z)$,

$$H(Z) = \left[1 - \sum_{k=1}^{K} A_k \, Z^{-k} \right], \tag{9}$$

or

$$\mathcal{E}(Z) = H(Z) \; X(Z). \tag{10}$$

Note that $H(Z)$ is a polynomial in Z which will have K roots or zero factors. Since "white" noise has a power spectrum known to be equal to a constant, then from Eq. (10) it is evident that we can solve for our unknown input power spectrum if the filter function is known, i.e.,

$$| X(\omega) |^2 = \frac{| \mathcal{E}(\omega) |^2}{| H(\omega) |^2} = \frac{\text{(constant)}}{\left| \prod_{k=1}^{K} (1 - D_k e^{-j\omega}) \right|^2}, \tag{11}$$

where the peaks (poles) of the unknown power spectrum will occur at the zeros of the filter function. This permits us to model the input sequence with the powerful, discrete, all-pole, linear prediction filter illustrated in Fig. 2, both in the frequency domain and in the time domain. The prediction filter is driven by white noise.

If one considers the action of such a filter upon sinusoids corrupted with a small amount of noise, it is evident that the filter can synchronize with even a short section of the sampled time waveform of the sinusoids and, once synchronized, can then proceed to "predict" many additional samples of the waveform with little error.

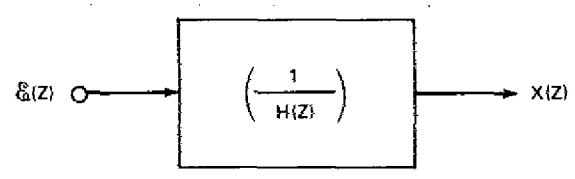

(a) Frequency domain

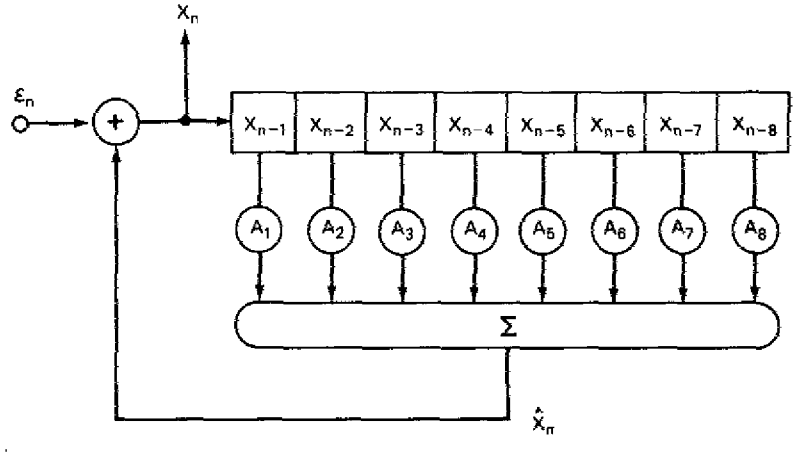

(b) Time domain

Fig. 2—Discrete all-pole linear prediction filter model

Another aspect of this filter is that it is a deconvolution filter, so-called because it estimates the unknown spectrum directly from the reciprocal of the filter transform function. Note in Eq. (10) that the error spectrum results from a simple multiplication of the unknown spectrum with the filter function, and that no convolution of the two occurs. In the conventional windowed Fourier transform method, on the other hand, the unknown spectrum is estimated by convolving the spectrum with the window filter transform function, and the convolution usually smears or destroys the fine detail of peaked spectra.

Reference 1 is recommended for those readers who want additional information on spectrum estimation filters.

LINEAR PREDICTION FILTERS AND ADAPTIVE SIDELOBE CANCELLERS

Conversion of the above MESA linear prediction filter to a weighted linear array of spatial sensors is straightforward, with the simplest configuration illustrated in Fig. 3. The element signal samples will be correlated in both space and time, giving rise to a two-dimensional data problem, but we convert this to spatial domain only by assuming that narrowband filtering precedes our spatial domain processing. For example, one could perform fast Fourier transform (FFT) on the element data prior to spatial processing. Also, we assume that our elements are equally spaced.

The nth "snapshot" signal sample at the kth element will consist of independent Gaussian receiver noise η_{kn} plus I incoherent source voltages,

$$E_{kn} = \eta_{kn} + \sum_{i=1}^{I} J_i e^{j(ku_i + \phi_{in})} \qquad 1 \leqslant k \leqslant K, \tag{12}$$

where

$u_i = 2\pi \left(\frac{d}{\lambda}\right) \sin \theta_i$

d = element spacing, assumed near $\lambda/2$

λ = wavelength

θ_i = spatial location angle of ith source

J_i = amplitude of ith source†

ϕ_{in} = random phase of ith source, nth sample

k = element index

n = snapshot sample index.

A "snapshot" is defined as one simultaneous sampling of the aperture signals at all array elements, and we assume that N snapshots of data are available.

†J_i has a constant rather than random amplitude because of a concurrent measurement program involving CW sources sampled at random times.

A brief examination of Fig. 3 from the standpoint of adaptive arrays leads to the conclusion that it is identical in configuration to a special subclass commonly referred to in the literature as a *sidelobe canceller* [13,14]. A typical sidelobe canceller configuration from Applebaum [14] is illustrated in Fig. 4. For the benefit of those who may not be familiar with them, it should be noted that the unweighted main-beam "element" is usually different and of much higher gain than the others, and the elements may or may not be equally spaced. They are designed to be operated on the basis of many successive snapshots (assuming digital operation) because their environment generally involves weak desired signals and an abundance of interference source data. They are a prediction filter in the sense that, after convergence, they are predicting the signal at the phase center of the main-beam element.

The adaptive sidelobe canceller is pertinent to our linear prediction filter because its spatial filter pattern analysis is well developed and can be applied directly to achieve a better understanding of the superresolution performance behavior. A further point is that real-time operation is readily achieved via most of the current adaptive algorithms, provided that the number of snapshots is enough to reach convergence in whitening ϵ. Convergence may require as few as two snapshots or as many as several thousand, depending on the particular algorithm and the parameters of the source distribution. Several examples will be discussed.

SPATIAL FILTER PATTERNS

The spatial filter function for the array of Fig. 3 is simply the adapted pattern after convergence, which is commonly referred to as the steady-state adapted pattern and may readily be computed from the inverse of the sample covariance matrix [14],

$$\mathbf{W}_o = \mu \mathbf{M}^{-1} \mathbf{S}^* \tag{13}$$

$$\mathbf{S}^{*t} = [0,0,0,0,0,0,0,1] \tag{14}$$

$$\mathbf{M} = \frac{1}{N} \sum_{n=1}^{N} \mathbf{M}_n \tag{15}$$

$$\mathbf{M}_n = \left[\mathbf{E}_n^* \cdot \mathbf{E}_n^t \right], \tag{16}$$

where $\mathbf{E}_n$ is the nth "snapshot" signal sample vector whose components are given by Eq. (12), $\mathbf{M}_n$ is the nth snapshot contribution to the covariance matrix, $\mathbf{M}$ is the sample covariance matrix averaged over N shapshots, $\mathbf{S}^*$ is the quiescent weight steering vector, μ is a scalar quantity, and $\mathbf{W}_o$ is the optimum weight vector. Note that the steering vector $\mathbf{S}^*$ injects zero weight on every element except for the end element, causing the quiescent pattern of the array to be that of the single end element.

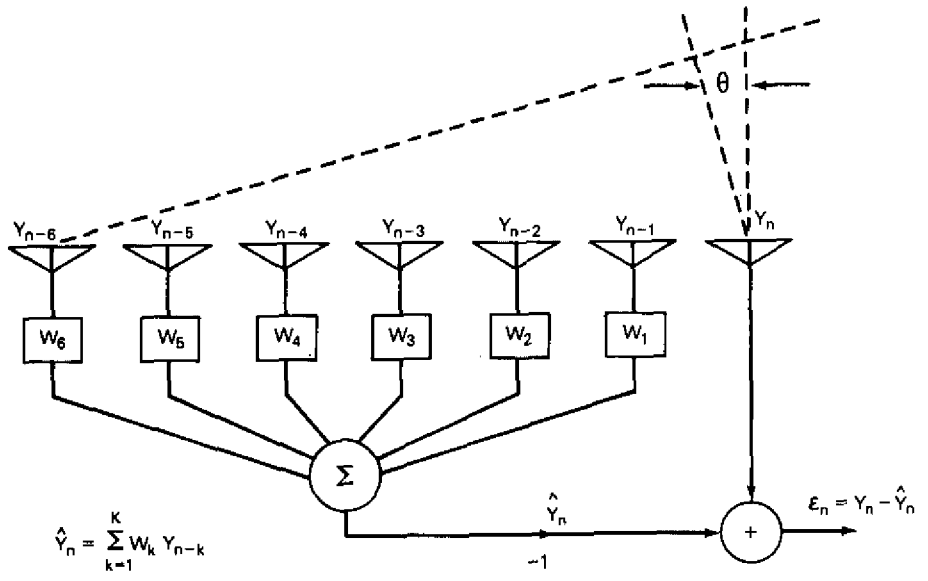

Fig. 3—Array aperture linear prediction spatial filter model

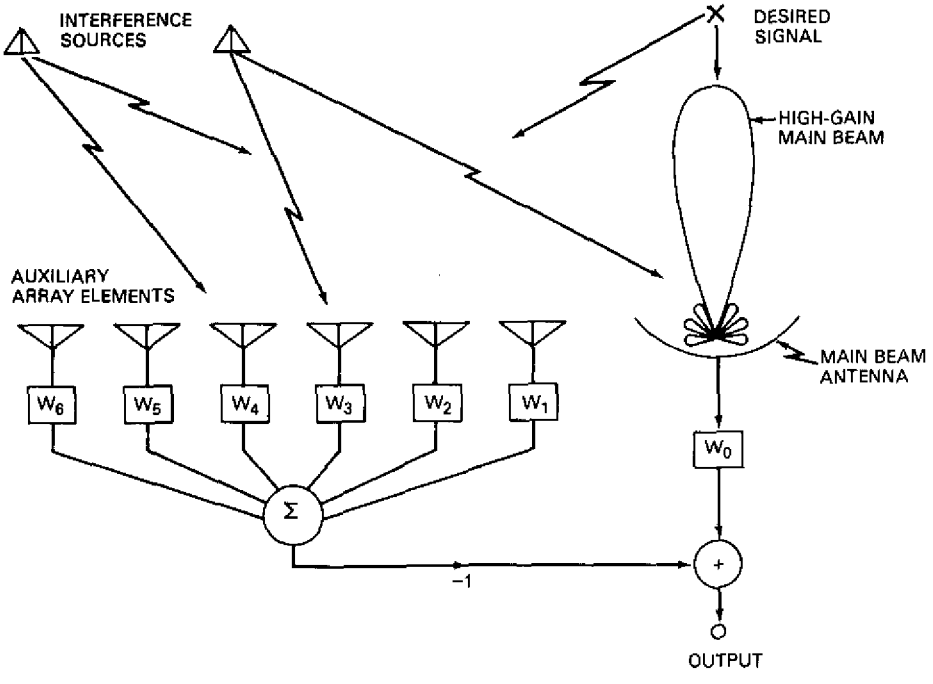

Fig. 4—Typical adaptive array sidelobe canceller configuration

Figure 5 shows a typical quiescent (single-element) pattern and an adapted pattern obtained from an 8-element linear array with two far-field, incoherent, 30-dB sources located at 18° and 22°. The adapted pattern weights were computed per Eq. (13) from the inverse of the covariance matrix averaged over 1024 simulated snapshots. Note that the two pattern nulls (zeros) align perfectly with the locations of the two sources. Of course, the array signals in this simulation were corrupted only by receiver noise (no element errors are included), and an average over 1024 snapshots is indeed steady state. Another important point to note is that nulls in such an adapted pattern may be located arbitrarily close together in terms of beamwidth, without violating any physical principle. Yet, because the nulls have served to locate two sources within a beamwidth, one may describe this as a "superresolution" pattern.

It is readily shown that this adapted pattern is obtained by subtracting the summed array output pattern from the element (main beam) pattern and, furthermore, that the summed array pattern consists of properly weighted "eigenvector beams" [15]. In terms of the eigenvector weights, we can express the optimum weights in the form,

$$\mathbf{W}_o = \mathbf{S}^* - \sum_{i=1}^{K} \left(\frac{B_i - B_o}{B_i + B_o} \right) \hat{\mathbf{W}}_{qi} \mathbf{e}_i \tag{17}$$

$$\hat{\mathbf{W}}_{qi} = \left(\mathbf{e}_i^{*t} \mathbf{S}^* \right)$$

where $\mathbf{e}_i$ is the ith eigenvector of the covariance matrix, B_i is the ith eigenvalue, and B_o is the smallest eigenvalue corresponding to receiver noise power. Note that only the significant eigenvectors corresponding to $B_i > B_o$ need be considered here. An adaptive array forms one such eigenvector beam for each degree of freedom consumed in nulling out the spatial source distribution. Figure 6 shows the two eigenvector beams required for this two-source example. It should be emphasized here that the true resolution and signal gain of the array are reflected in these eigenvector beams. They demonstrate the importance of having as wide an aperture as possible because the superresolution capability in the adapted pattern is a percentage of the true resolution of these beams. Also, since the superresolution nulls are formed by subtracting these beams of conventional width, it follows that the nulls will be rather delicate and very sensitive to system imperfections and signal fluctuations.

The desired "spatial spectrum pattern" is then obtained from Eq. (11) as simply the inverse of the adapted pattern. Figure 7 shows this inverse for the two-source example and compares it with the output of a conventional beam scanned through the two sources. Several comments are in order concerning such inverse patterns.

1. They are not true antenna patterns because there is no combination of the element weights that could produce such a peaked spatial pattern. They are simply a function computed from the reciprocal of a true antenna pattern.

2. Linear superposition does not hold in either the inverse or the original adapted pattern because of the nonlinear processing involved in the inverse of the covariance matrix (or the equivalent).

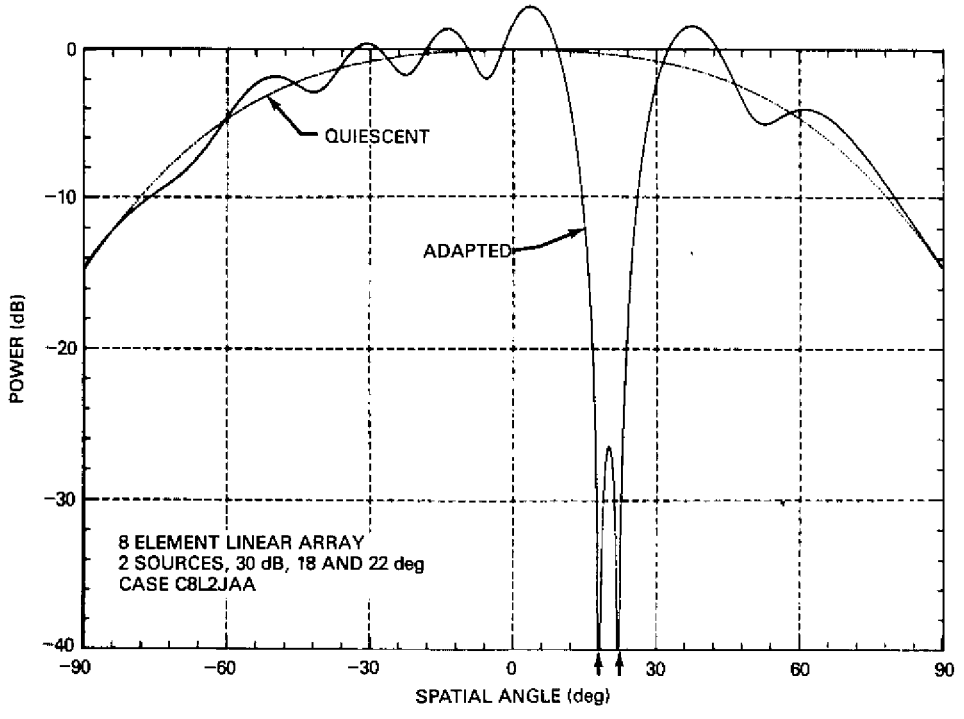

Fig. 5—Quiescent (single-element) and adapted patterns for two-source case, covariance matrix inverse algorithm, 1024 datasnaps

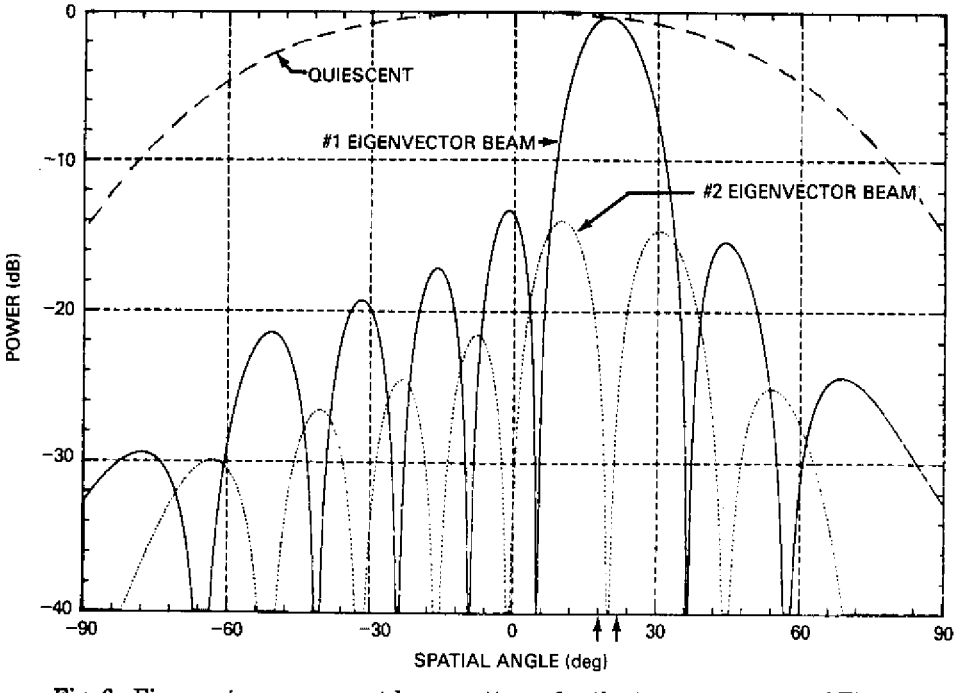

Fig. 6—Eigenvector component beam patterns for the two-source case of Fig. 5

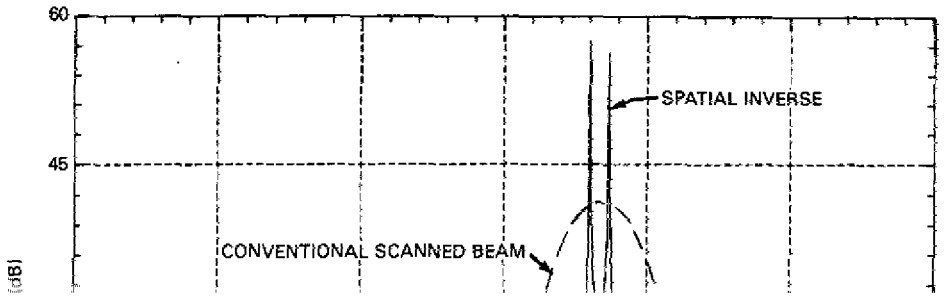
60
45
SPATIAL INVERSE
CONVENTIONAL SCANNED BEAM
(dB)

REAL-TIME FILTER OPERATION

To get a feel for real-time operation performance with realistic weight update averaging, we ran simulations in which an eight-element array had its weights computed from the simple Howells—Applebaum algorithm in recursive digital form as diagrammed in Fig. 8. The associated recursive relationship for the kth weight may be written

$$(1 + \tau)\, W_k(n) = \tau W_k(n-1) + S_k^*(n) - \left(\frac{1}{B_o}\right) E_k^*(n)\, Y(n) \tag{18}$$

where

$$Y(n) = \sum_{k=1}^{K} E_k(n)\, W_k(n-1). \tag{19}$$

$Y(n)$ is the current array output, $E_k(n)$ is the current snapshot signal sample at the kth element (similar to Eq. (12)), $W_k(n\text{-}1)$ is the previous value of the kth weight, $S_k^*(n)$ is the injected kth beam-steering weight, and B_o is a constant equal to receiver noise power.

The digital integration loop shown in Fig. 8 is designed to simulate a simple low-pass RC filter with a time constant of τ, but we choose to make τ dynamic to get faster convergence for most situations. Thus, let τ become $\tau(n)$,

$$\tau(n) = \tau_o + TP_r(n) \tag{20}$$

where

T = high-power, fast time constant

τ_o = quiescent conditions, slow time constant

$P_r(n)$ = snapshot SNR (power ratio).

This formulation permits us to satisfy the 10% bandwidth criterion at high power levels to avoid noisy weights [15] by choosing the value of $T = 3.2$, and yet the quiescent condition time constant need be no worse than $\tau_0 = 200$. The larger value for τ_0 is necessary in order to have a relatively stable quiescent pattern. Actual weight update averaging is performed in accordance with the reciprocal of the closed-loop bandwidth α,

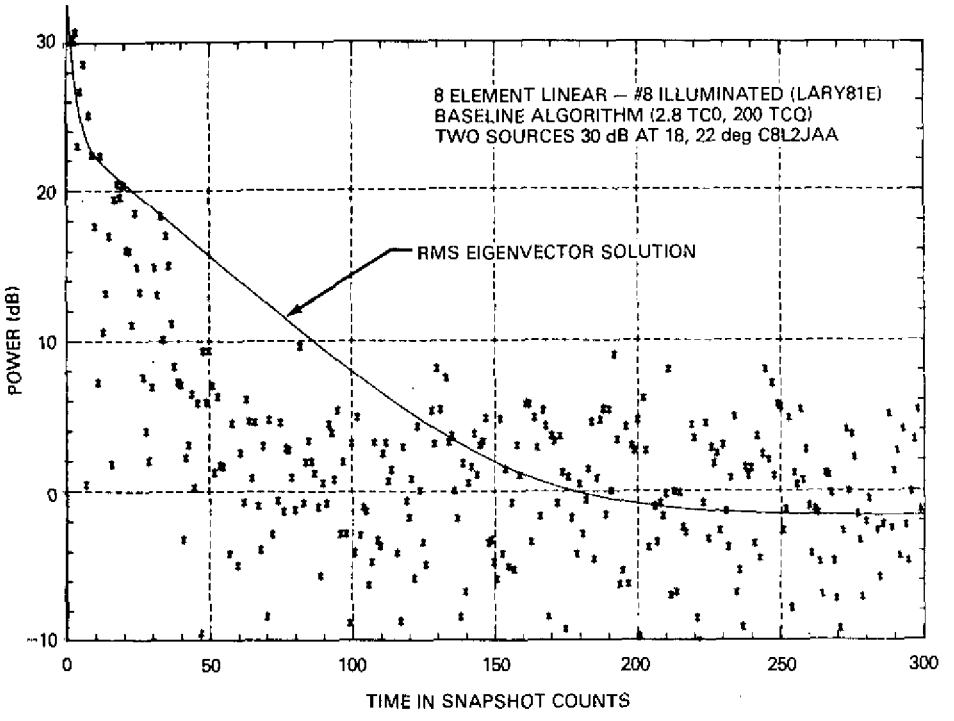

Fig. 9—Time-sequence snapshot output of array in decibels above receiver noise power; Howells-Applebaum recursive algorithm with dynamic time constant

any of the snapshot weight sets can be used to compute the spatial spectrum. Figure 10 shows the spatial spectrum plots associated with snapshots 100, 200, and 300. In comparing Fig. 10 against Fig. 7, note that the pattern has changed very little, in spite of the fact that the integration or averaging has been reduced by two orders of magnitude, i.e., from a value of 1024 snapshots in Fig. 7 to about 3 snapshots in Fig. 10 (albeit a decaying average inherent in the low-pass filter). The greatest effect of this reduced averaging is that the heights of the peaks are reduced and the peaks fluctuate from snapshot to snapshot because of the perturbation of the noise on each snapshot weight update.

In rounding out the example of these two incoherent sources spaced 4° apart (about 0.27 beamwidths apart), Fig. 11 illustrates what happens as we reduce the SNR strength of the sources. Figure 11a at 20 dB shows increasing peak fluctuations in magnitude, which merely reflect the null fluctuations in the adapted pattern, although the spatial locations of the sources are still accurate. Figure 11b at 10 dB shows even greater fluctuations in peak magnitude, but now the patterns are deteriorating in both shape and peak locations, indicating that the resolution capability is nearing its limit, i.e., if the source power levels are reduced further, then the adaptive array can no longer resolve them accurately at that particular spacing.

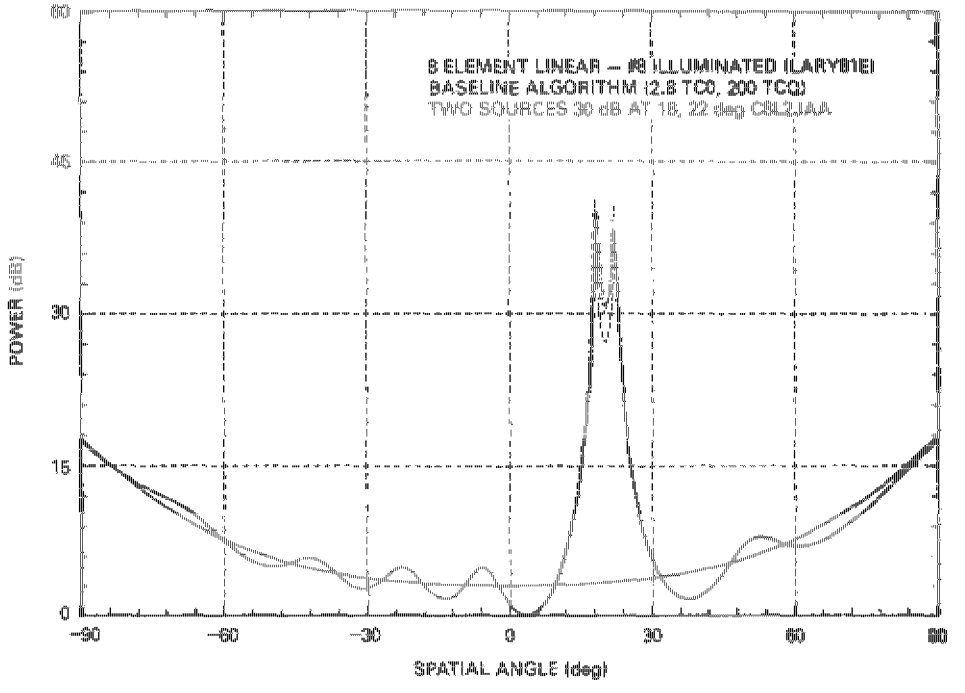

Fig. 10—Typical spatial spectrum snapshot plots after convergence, snapshot weight sets 100, 200, and 300. Two 30-dB sources were located at 18° and 22°.

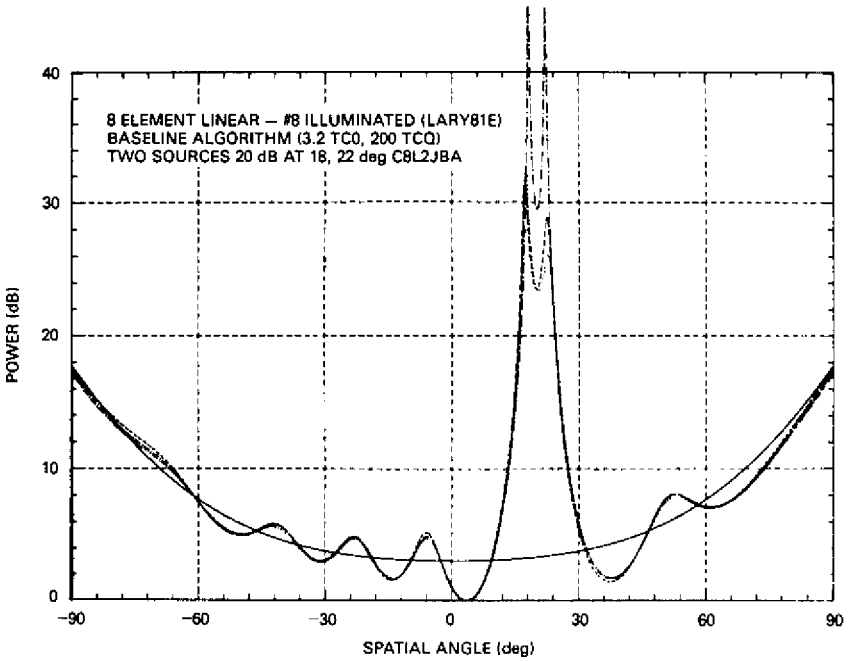

(a) 20-dB SNR sources

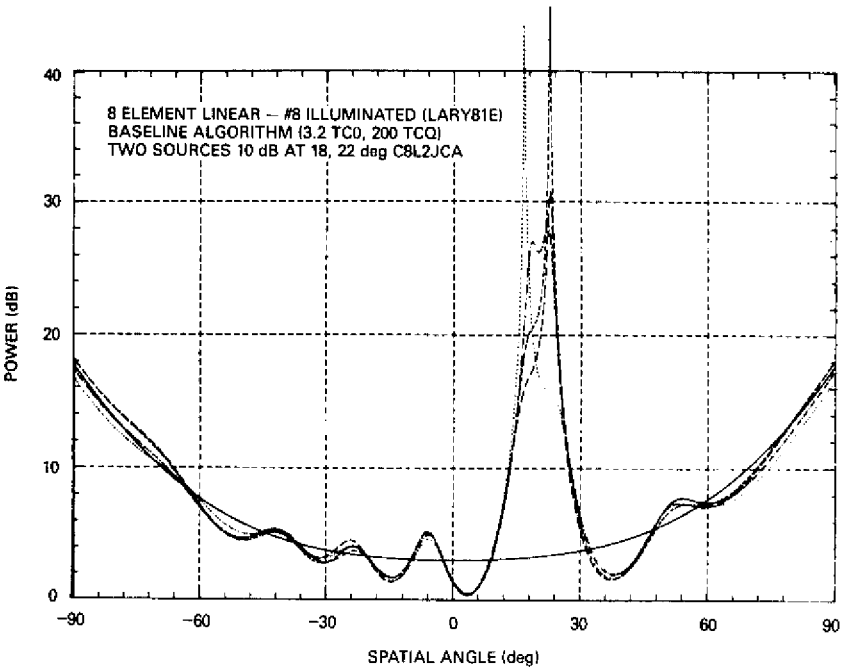

(b) 10-dB SNR sources

Fig. 11—Typical spatial spectrum snapshot plots after convergence. Two sources located at 18° and 22°

described by Alam [11,17]. Figure 13 shows the resolution of the three sources via the Gram—Schmidt algorithm, but it should be noted that, even with this fast algorithm, resolution was not achieved until after 200 snapshots and the locations of the peaks fluctuates considerably. This was a good illustration of the "delicacy" of null formation for the case of closely spaced multiple sources.

MLM AND ADAPTIVE DIRECTIONAL CONSTRAINTS

The maximum likelihood spectral estimate is defined as a filter designed to pass the power in a narrow band about the signal frequency of interest and minimize or reject all other frequency components in an optimal manner [4,5]. This is identical to the use of a zero-order main-beam directional gain constraint in adaptive arrays [18,19], where the "spatial spectrum" would be estimated by the output residual power P_o from the optimized adapted array weights,

$$P_o = \mathbf{W}_o^{*t} \mathbf{M} \mathbf{W}_o \tag{22}$$

where

$\mathbf{W}_o$ = $\mu \mathbf{M}^{-1} \mathbf{S}^*$(optimized weights)

$\mathbf{M}$ = covariance matrix estimate

$\mathbf{S}^*$ = main-beam direction-steering vector

μ = scalar quantity.

Under the zero-order gain constraint, we require $\mathbf{S}^t \mathbf{W}_o = 1$, whereupon μ becomes

$$\mu = (\mathbf{S}^t \mathbf{M}^{-1} \mathbf{S}^*)^{-1}. \tag{23}$$

Substituting μ and $\mathbf{W}_o$ into Eq. (22), then, results in

$$P_o = \frac{1}{\mathbf{S}^t \mathbf{M}^{-1} \mathbf{S}^*} \quad . \tag{24}$$

Upon sweeping the steering vector $\mathbf{S}^*$ for a given covariance matrix inverse, P_o will estimate the spatial spectrum. Interestingly, this result is identical (within a constant) to the spectrum obtained from the *inverse* of the output residual power from an unconstrained optimized adapted array.

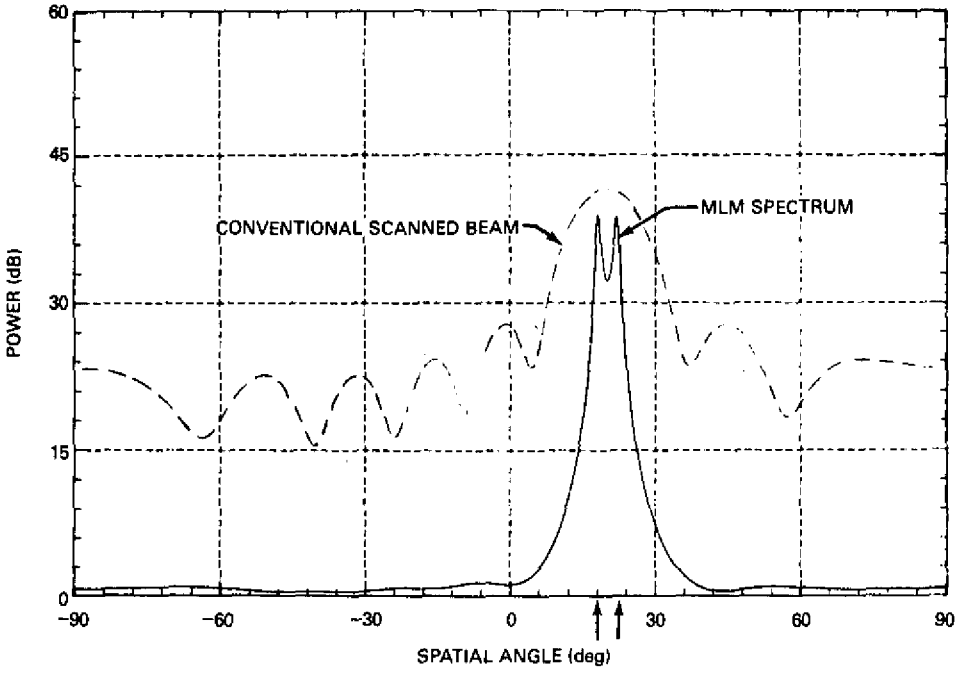

Fig. 14—MLM spatial spectrum plotted from residual power of adaptive zero-order main-beam constraint for the two-source case of Fig. 5

3. The output of this filter is a real signal, and if the filter passband is steered to a particular source, one can monitor that source at full array gain while rejecting outputs of all other sources.

4. The residual background spatial ripple is very low and well behaved.

5. It is not necessary to have the elements equally spaced. Thus, one should take advantage of this property to spread them out for a wider aperture and substantially increase the resolution for a given number of elements. (This is done in the field of geophysics [4].) If this is done, it is very likely that this method could equal or surpass the resolution of the previous technique.

ALTERNATE ADAPTIVE PROCESSING FOR SPATIAL SPECTRA

Phase Center Prediction

The adaptive array processing described in the fourth section did not use the configuration of Fig. 3 in the true sense of a K-point linear prediction filter that runs across a larger aperture of data samples. The K elements involved were the total aperture, and a series of N snapshots of data were used to estimate or predict the signal at the phase center of the unweighted main-beam element. Phase-center prediction of this type is very flexible in that

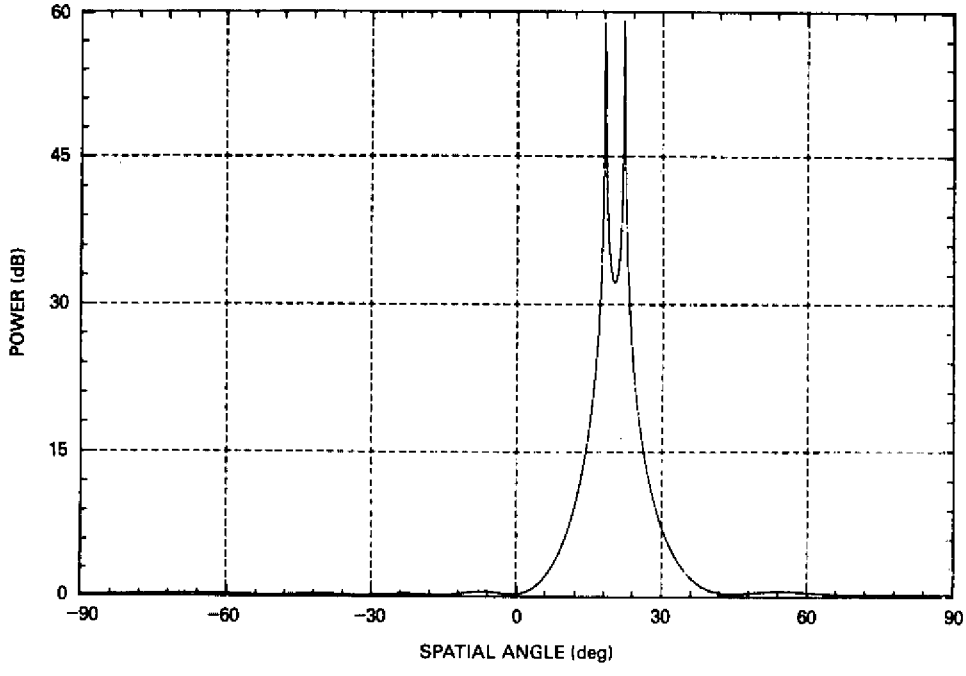

Fig. 15—"Thermal noise" algorithm spatial spectrum plotted for the two-source case of Fig. 5

SIGNIFICANT PROCESSING DIFFERENCES

Although the similarities are extensive enough to create a favorable climate for technique interchanges, there are also some significant differences which arise from the very nature of the applications and their data. For example, assume that we utilize the Burg MESA technique to run a K-point prediction filter across an RF aperture of M elements, where K must be smaller than M by at least 50% in order to obtain a reasonable averaged estimate for determination of the K filter weights. This type of processing has a great advantage in being able to operate with a single snapshot of element data, but it is "unthinkable" from an RF array point of view because it is wasting expensive aperture elements. It is far more preferable to operate on the basis of many snapshots of data from the smallest number of elements possible. In fact, a recent study of the Burg MESA technique by King [8], as applied to an RF spatial array, found that single snapshot results were seldom satisfactory, and that it was usually necessary to average the results from 10 or 20 snapshots in order to achieve a stable spectrum estimate. This comment is not meant to imply that the Burg technique is not applicable, but only that single-snapshot operation is not very practical for RF arrays.

A related difference is simply the fact that RF array element signal samples are correlated in both space and time, thus giving rise to a two-dimensional data problem [7] that does not exist in spectrum analysis. To overcome this problem usually requires filtering in both domains. For example, one may handle the time domain via tapped delay lines, an FFT operation, or actual narrowband filters at each array element. Note that, in each case,

The adaptive array counterpart is naturally suited to real-time spectral estimation via most of the current adaptive algorithms, and the case of two incoherent sources located within a beamwidth was simulated over a SNR range of 0 to 40 dB. A universal super-resolution performance curve, Fig. 12, was developed for this particular case, which can be utilized for linear arrays of any number of elements. If there are more than two sources within a beamwidth, difficulties mount rapidly and the filter null points may not accurately represent source locations.

In addition to the direct adaptive counterparts, two alternate adaptive spatial spectrum estimators were suggested. One is a circular array aperture arrangement which predicts to the center of the circle, and the other is a new adaptive "thermal noise" algorithm which appears to possess an interesting combination of both MESA and MLM characteristics.

There are some significant differences between spectral analysis techniques and adaptive array techniques that relate to the nature of their applications and the two-dimensional data problem. However, it appears that there is much to be gained through careful analysis of the other's techniques. For example, in addition to the obvious applications in target detection, DF (direction finding) systems, and source classification, spectral analysis techniques should be of benefit in data extension and coherence effects investigations.

REFERENCES

1. *Modern Spectrum Analysis*, D. G. Childers, ed., IEEE Press, New York, 1978. (Note: This book contains complete copies of references 2—7, 9, 11, 12.)

2. J. P. Burg, "Maximum Entropy Spectral Analysis," in *Proc. 37th Meeting of the Society of Exploration Geophysicists*, 1967, Oklahoma City.

3. J. P. Burg, "A New Analysis Technique for Time Series Data," Paper presented at the NATO Advanced Study Institute on Signal Processing with Emphasis on Underwater Acoustics, Enschede, Netherlands, 1968.

4. J. Capon, "High-Resolution Frequency-Wavenumber Spectrum Analysis," *Proc. IEEE* 57, 1408—1418 (Aug. 1969).

5. R. T. Lacoss, "Data Adaptive Spectral Analysis Methods," *Geophysics* 36, 661—675 (Aug. 1971).

6. J. P. Burg, "The Relationship between Maximum Entropy Spectra and Maximum Likelihood Spectra," *Geophysics* 37, 375—376 (Apr. 1972).

7. R. N. McDonough, "Maximum-Entropy Spatial Processing of Array Data," *Geophysics* 39, 843—851 (Dec. 1974).

8. W. R. King, "Maximum Entropy Wavenumber Analysis," NRL Report 8298, Mar. 1979.

ent of Digital Instantaneous Frequency," *IEEE Trans.*

eal-Time Adaptive Linear Prediction Using the Least
," *IEEE Trans.* ASSP-24, 494–507 (Dec. 1976).

Estimation," in *Proc. 1977 Joint Automatic Control*
, Calif.

rpretation of Maximum Entropy Spectral Analysis,"
ly 1971).

Fixed and Adaptive Resolution at GE and SURC,"
ept. 1976).

ays," *IEEE Trans.* AP-24, 585–598 (Sept. 1976).

–An Introduction," *Proc. IEEE* 64, 239–272 (Feb.

. Brennan, "Rapid Convergence Rate in Adaptive
53–863 (Nov. 1974).

ce Filter—A Multistage Multichannel Estimation
8–1383 (Dec. 1978).

or Linearly Constrained Adaptive Array Processing,"
1972).

nan, "Adaptive Arrays with Main Beam Constraints,"
ept. 1976).

NRL Formal Report 8345

Nonlinear Spectral Analysis and Adaptive Array Superresolution Techniques

William F. Gabriel

February 1, 1980

NAVAL RESEARCH LABORATORY
Washington, D.C.